THE ASTROPHYSICAL JOURNAL, 438:887–903, 1995 January 10

HYDRODYNAMICS OF BINARY COALESCENCE. II. POLYTROPES WITH $\Gamma = 5/3$

FREDERIC A. RASIO[1]
Institute for Advanced Study, Olden Lane, Princeton, NJ 08540
E-mail: rasio@guinness.ias.edu

AND

STUART L. SHAPIRO[2]
Center for Radiophysics and Space Research, Cornell University, Ithaca, NY 14853
Received 1994 April 4; accepted 1994 July 15

ABSTRACT

We present a new numerical study of the equilibrium and stability properties of close binary systems. We use the smoothed-particle hydrodynamics (SPH) technique both to construct accurate equilibrium configurations in three dimensions and to follow their hydrodynamic evolution. We adopt a simple polytropic equation of state $p = K\rho^{\Gamma}$ with $\Gamma = 5/3$ and $K =$ constant within each star, applicable to low-mass degenerate dwarfs as well as low-mass main-sequence stars. For degenerate configurations, we set the two polytropic constants equal, $K = K'$, independent of the mass ratio. For main-sequence stars, we adjust K and K' so as to obtain a simple mass-radius relation of the form $R/R' = M/M'$, where R' and M' are the radius and mass of the secondary. Along a sequence of binary equilibrium configurations for *two identical stars*, we demonstrate the existence of both secular and dynamical instabilities, confirming directly the results of recent analytic work. We use the SPH method to calculate the nonlinear development of the dynamical instability and to determine the final fate of the system. We find that the two stars merge together into a single, rapidly rotating object in just a few orbital periods. Equilibrium sequences are also constructed for systems containing *two nonidentical stars*. These sequences terminate at a Roche limit, which we can determine very accurately using SPH. For two low-mass main-sequence stars with mass ratio $q \lesssim 0.4$ we find that the (synchronized) Roche limit configuration is secularly unstable. For $q \lesssim 0.25$, a dynamical instability is encountered before the Roche limit. Degenerate binary configurations remain hydrodynamically stable all the way to the Roche limit for all mass ratios $q \neq 1$. However, unstable mass transfer can occur beyond the Roche limit, and this is indeed observed in our numerical simulations. Dynamically unstable mass transfer also leads to the rapid coalescence of the binary system, although the details of the hydrodynamic evolution are quite different compared to that of an unstable equilibrium. We discuss the implications of our results for the evolution of double white-dwarf systems and W Ursae Majoris binaries.

Subject headings: binaries: close — hydrodynamics — instabilities — stars: interiors — stars: white dwarfs

1. INTRODUCTION AND MOTIVATION

Essentially all modern studies of close binary systems are done in the Roche approximation, where the noncompact components are modeled as massless gas in hydrostatic equilibrium in the effective potential of a point-mass system (see, e.g., Kopal 1978). This model applies well to very compressible objects with centrally concentrated mass profiles, such as giants and early-type main-sequence stars. In contrast, most of the classical work on close binaries was done in the completely opposite limit of a self-gravitating *incompressible* fluid (see Chandrasekhar 1969, and references therein; see also Hachisu & Eriguchi 1984b). An essential result found in the incompressible case is that the hydrostatic equilibrium solutions for sufficiently close binaries can become *globally unstable* (Chandrasekhar 1975; Tassoul 1975). Using numerical hydrodynamic calculations, Rasio & Shapiro (1992, hereafter RS) demonstrated that these instabilities persist in the compressible regime, at least down to an adiabatic index as low as $\Gamma = 2$ for two identical polytropes.

A *dynamically* unstable binary coalesces in just a few orbital periods, forming a rapidly rotating spheroidal object surrounded by a thick disk of shock-heated material (RS). But well before a close binary system becomes dynamically unstable (and even if it never does), another type of global instability can affect its evolution. It has been referred to by various names, such as secular instability (Lai, Rasio, & Shapiro 1993a, 1994b), tidal instability (Counselman 1973; Hut 1980), gravogyro instability (Hachisu & Eriguchi 1984a), and Darwin instability (Levine et al. 1993). Its physical origin is easy to understand (Lai et al. 1993a, 1994b; Rasio 1994). There exists a *minimum* value of the total angular momentum J for a *synchronized* close binary. This is simply because the spin angular momentum, which *increases* as r decreases for a synchronized system, can become comparable to the orbital angular momentum for sufficiently small r. A system that reaches the minimum of J cannot evolve further by angular momentum loss and remain synchronized. Instead, the combined action of tidal forces and viscous dissipation will drive the system *out* of synchronization and cause rapid orbital decay as angular momentum is continually transferred from the orbit to the spins.

The classical analytic studies for binaries containing an incompressible fluid (Chandrasekhar 1969) were recently extended to polytropes in the work of Lai, Rasio, & Shapiro (1993a, b, 1994a, b, c, hereafter LRS1–5 or collectively LRS). The approach of LRS is based on the use of an energy varia-

[1] Hubble Fellow.
[2] Departments of Astronomy and Physics, Cornell University.

tional principle to construct approximate equilibrium configurations and study their stability. The stars are modeled as self-gravitating compressible ellipsoids, and the tidal interaction is truncated to quadrupole order. Instabilities are identified simply from turning points appearing along sequences of equilibrium configurations. Both secular *and dynamical* instabilities can be identified in this way (LRS1). Some applications to the problem of binary coalescence have been discussed in LRS2 and LRS3. In LRS5, the method was extended to treat the *dynamical* evolution of compressible ellipsoids. The great usefulness of an analytic approach lies in its simplicity. Using the method of LRS, one can obtain an equilibrium model by solving a set of algebraic equations, a task that can be performed on a workstation in seconds. The dynamical evolution of binary systems can be calculated approximately by solving ordinary differential equations (LRS5). As a result, it is possible to explore a wide variety of simple models. In addition, an analytic treatment can provide physical insight into difficult issues of global stability that are easily missed when using multidimensional numerical calculations.

There are, however, obvious limitations to an analytic treatment. While linear stability can be investigated and orbital decay can be tracked prior to contact, the final fate of unstable systems remains unknown. Quantitative accuracy is limited by the use of approximate trial functions in a variational formulation. Stability limits obtained from a variational principle give, at best, sufficient conditions for instability (Bardeen et al. 1977; Hunter 1977). In the method of LRS, quantitative accuracy can be poor when the binary configuration is close to contact or when the compressibility of the fluid is high. In some cases, qualitatively incorrect or unphysical results can even be obtained (see LRS4, § 5).

Coalescing binaries and stellar mergers are associated with a number of topical problems in astrophysics. The design of the gravitational-wave detectors for the LIGO project (Abramovici et al. 1992) is based largely on theoretical models for the coalescence of two neutron stars. The final stage of this coalescence, when the two neutron stars merge hydrodynamically, produces a burst of gravitational radiation whose characteristics probe directly the interior structure of a neutron star. In Paper I (Rasio & Shapiro 1994), we used simple polytropic models of binary neutron stars to study the hydrodynamics of their final coalescence and the corresponding emission of gravitational waves. Since the nuclear equation of state at high densities is rather stiff, we adopted high values of the adiabatic index, $\Gamma \gtrsim 2$ (polytropic index $n \lesssim 1$). Here, in contrast, we consider polytropes with $\Gamma = 5/3$ ($n = 3/2$). These represent fairly good models of low-mass white dwarfs and main-sequence stars. For white dwarfs, the mass must be $\lesssim 1\ M_\odot$, so that the degenerate electrons are essentially nonrelativistic (e.g., Shapiro & Teukolsky 1983). For main-sequence stars, we must have $M \lesssim 0.5\ M_\odot$, so that most of the mass is contained in the convective envelope (cf. LRS4, Table 3; Kippenhahn & Weigert 1990, § 22.3).

Coalescing white dwarf binaries are now thought to be the likely progenitors of Type Ia supernovae (Iben & Tutukov 1984; Webbink 1984; Paczyński 1985; Yungleson et al. 1994). To produce a supernova, the total mass of the system must be above the Chandrasekhar mass. Given evolutionary considerations, this requires two C-O or O-Ne-Mg white dwarfs. Yungelson et al. (1994) show that the expected merger rate for close pairs of white dwarfs with total mass exceeding the Chandrasekhar mass is consistent with the rate of Type Ia supernovae deduced from observations. Alternatively, a massive enough merger may collapse to form a rapidly rotating neutron star (Nomoto & Iben 1985; Colgate 1990). Chen & Leonard (1993) have discussed the possibility that most millisecond pulsars in globular clusters may have formed in this way. In some cases planets may form in the disk of material ejected during the coalescence and left in orbit around the central pulsar (Podsiadlowski, Pringle, & Rees 1991). Objects of planetary masses in orbit around a millisecond pulsar (PSR B1257+12) have indeed been detected (Wolszczan 1994). A merger of two highly magnetized white dwarfs might lead to the formation of a neutron star with extremely high magnetic field, and this scenario has been proposed as a source of gamma-ray bursts (Usov 1992).

Close white dwarf binaries are expected to be extremely abundant in our Galaxy. Iben & Tutukov (1984, 1986) predict that $\sim 20\%$ of all binary stars produce close pairs of white dwarfs at the end of their stellar evolution. The most common systems should be those containing two low-mass helium white dwarfs. Their final coalescence can produce an object massive enough to start helium burning. Bailyn (1993) suggests that extreme horizontal branch stars in globular clusters may be such helium-burning stars formed by the coalescence of two white dwarfs. Paczyński (1990) has proposed that the peculiar X-ray pulsar 1E 2259+586 may be the product of a recent white dwarf merger. Planets in orbit around a massive white dwarf may also form following a merger (Livio, Pringle, & Saffer 1992).

Close double white dwarfs are also very important sources of low-frequency gravitational waves that should be easily detectable by future space-based interferometers. Recent proposals for space-based interferometers include the LAGOS experiment (Stebbins et al. 1989), which should have an extremely high sensitivity (down to an amplitude $h \sim 10^{-23}$ to 10^{-24}) to sources with frequencies in the range ~ 0.1–100 mHz. Evans, Iben, & Smarr (1987) estimate a white dwarf merger rate of order one every 5 yr in our own Galaxy. Coalescing systems closest to Earth should produce quasi-periodic gravitational waves of amplitude $h \sim 10^{-21}$ in the frequency range ~ 10–100 mHz. In addition, the total number ($\sim 10^4$) of close white dwarf binaries in our Galaxy emitting at lower frequencies ~ 0.1–1 mHz (the emission lasting for $\sim 10^2$–10^4 yr before final coalescence) should provide a continuum background signal of amplitude $h_c \sim 10^{-20}$ to 10^{-21}. Individual sources should be detectable by LAGOS above this background when their frequency becomes $\gtrsim 10$ mHz. The detection of the final burst of gravitational waves emitted during the actual merging would provide a unique opportunity to observe in "real time" the hydrodynamic interaction between the two white dwarfs, possibly followed immediately by a supernova explosion, nuclear outburst, or some other type of electromagnetic signal.

Main-sequence stars in the process of merging (or about to merge) are directly observed as W Ursae Majoris contact systems (see Rucinski 1992 for a recent review). The question of the interior structure of these contact systems has been the subject of a heated debate (see Shu 1980 for a summary) and remains unresolved. At least some of the blue stragglers observed in stellar clusters must be produced by the coalescence of two low-mass main-sequence stars in a close binary. Indeed, Mateo et al. (1990; see also Mateo 1993; Yan & Mateo 1994) and Kałużny & Krzeminski (1993) have found a number of W UMa–type contact binaries among the blue

stragglers in several globular clusters. Large numbers of contact binaries have also been found in open clusters (Kałużny & Rucinski 1993). Hydrodynamic processes occurring during the final coalescence of these binaries must play an essential role in determining the properties of blue stragglers (Bailyn & Pinsonneault 1994; Rasio 1993).

Our paper is organized as follows. In § 2 we review briefly our numerical method and general conventions. In § 3 we present our results for the equilibrium and stability properties of binary systems containing two identical stars. The dynamical evolution to complete coalescence is followed for several unstable systems. Binaries with mass ratio $q \neq 1$ are treated in § 4. We consider both the stability of equilibrium configurations up to the Roche limit and the stability of mass transfer following Roche lobe overflow. The implications of our results for various types of astrophysical systems are discussed in § 5.

2. NUMERICAL METHOD AND CONVENTIONS

We use the smoothed particle hydrodynamics (SPH) method for the numerical calculations presented here. Details about our implementation of SPH, as well as the results of a number of test calculations and comparisons with other numerical work are given in Paper I and RS. All calculations have been performed with $N \approx 4 \times 10^4$ particles, each particle interacting with a nearly constant number of neighbors $N_N \approx 64$. The gravitational field is calculated in three dimensions on a 256^3 Cartesian grid. With these resources, equilibrium configurations can be constructed that satisfy the virial theorem to within $\lesssim 10^{-3}$ (cf. Paper I, § 2.3, and Fig. 1). Dynamical integrations conserve total energy to within $\sim 10^{-2}$ and angular momentum to within $\sim 10^{-4}$.

Throughout this paper, numerical results are given in units where $G = M = R = 1$, where M and R are the mass and radius of the *unperturbed* (spherical) primary (i.e., the more massive of the two stars). The units of time, velocity, and density are then

$$t_0 = 1600 \text{ s} \times (R/R_\odot)^{3/2}(M/M_\odot)^{-1/2} , \quad (1)$$

$$v_0 = 440 \text{ km s}^{-1} \times (R/R_\odot)^{-1/2}(M/M_\odot)^{1/2} , \quad (2)$$

$$\rho_0 = 6 \text{ g cm}^{-3} \times (R/R_\odot)^{-3}(M/M_\odot) . \quad (3)$$

The mass of the secondary is denoted by $M' \leq M$, and the mass ratio is defined as $q = M'/M \leq 1$. For degenerate configurations, the equilibrium radius R' of the secondary is calculated assuming constant specific entropy throughout the system, i.e., we use the same polytropic constant $K = P/\rho^{5/3} = K' = P'/\rho'^{5/3}$ for both components when constructing initial conditions. This gives the equilibrium mass-radius relation $(R/R') = (M/M')^{-1/3}$. To model binaries containing low-mass main-sequence stars, we calculate $K' \leq K$ such that the approximate mass-radius relation $R/R' = M/M'$ is satisfied.

Particular problems are posed by the construction of accurate equilibrium configurations and the dynamical integrations for binaries with mass ratio q far from unity (as in § 4.1 below). As in Paper I, we use a *constant number density* of SPH particles with unequal masses to set up our initial conditions. Thus most of the particles are used to model the component of larger *volume*. This is an excellent way of maintaining good spatial resolution near the surface of a component about to fill its critical potential lobe. Indeed, in a system with $q \neq 1$, it is normally the star with the larger volume that will fill its critical lobe first (see § 4). Our method allows not only the accurate determination of the Roche limit along an equilibrium sequence, but also an accurate treatment of dynamical mass transfer. This is because a reasonably large number of SPH particles is always available near the inner Lagrangian point to feed the accretion flow, even if the mass density there is very low. A minor drawback of this approach is that a component with very small volume may have to be modeled using a very small number of SPH particles. For extreme cases, the more compact of the two stars may have to be modeled as a single point mass (we do not treat such extreme cases in this paper).

3. BINARIES WITH TWO IDENTICAL COMPONENTS

3.1. *Equilibrium and Secular Stability Properties*

Using the relaxation method at fixed binary separation r described in Paper I (§ 2.3), we have constructed very carefully a sequence of hydrostatic equilibrium configurations for two identical polytropes with $\Gamma = 5/3$. In all cases we calculate the self-gravity of the fluid directly in three dimensions (solving Poisson's equation by a grid-based FFT algorithm; see RS), without making any assumptions about the density profiles or about the smallness of the ratio R/r. In all cases our hydrostatic equilibrium solutions satisfy the virial theorem,

$$2T + 3(\Gamma - 1)U + W = 0 , \quad (4)$$

where

$$T = \frac{1}{2}\sum_i m_i v_i^2 , \quad U = \frac{1}{\Gamma - 1}\sum_i m_i A_i \rho_i^{\Gamma - 1} ,$$

$$W = \frac{1}{2}\sum_i m_i \Phi_i , \quad (5)$$

to better than one part in 10^3 (cf. Fig. 1 of Paper I). Here m_i and v_i are the mass and velocity of an individual SPH particle, ρ_i is the local density, Φ_i is the gravitational potential, $A_i = p_i/\rho_i^\Gamma$ is the entropy variable (here equal to the polytropic constant K), and the sums are over all SPH particles.

Some representative solutions along the equilibrium sequence are shown in Figure 1. The structure of these solutions is shown both in real space (projection onto the orbital x-y plane), and in terms of how the fluid fills the effective potential wells. For a synchronized (uniformly rotating) system with orbital frequency $\Omega_{\rm orb}$, we calculate the effective potential as

$$\Phi_e(x, y, z) = \Phi(x, y, z) - \tfrac{1}{2}\Omega_{\rm orb}^2(x^2 + y^2) , \quad (6)$$

where x is along the binary axis, z is along the rotation axis, and the origin is at the center of mass of the system. For fixed x, Φ_e is minimum on the binary axis ($y = z = 0$), and this minimum value is shown as a solid line in Figure 1. The fluid fills up the space above this line, up to a level $\Phi_e^{(s)}$ which is independent of x in hydrostatic equilibrium.[3] Along the binary axis the effective potential has a local maximum $\Phi_e^{(i)}$ at $x = 0$ (the inner Lagrangian point) and global maxima $\Phi_e^{(0)}$ at $|x| = x_0$ (the outer Lagrangian points). There are two minima at $|x| = x_c$, corresponding to the centers of the two components.[4]

[3] The value of Φ_e for SPH particles very close to the true fluid surface is only approximately constant, as seen in Fig. 1. This is because the *number density* of SPH particles is not exactly constant around the surface of a star with a large tidal deformation.

[4] Note that in general $r \neq 2x_c$, since we define the binary separation r as the distance between the *centers of mass* of the two components.

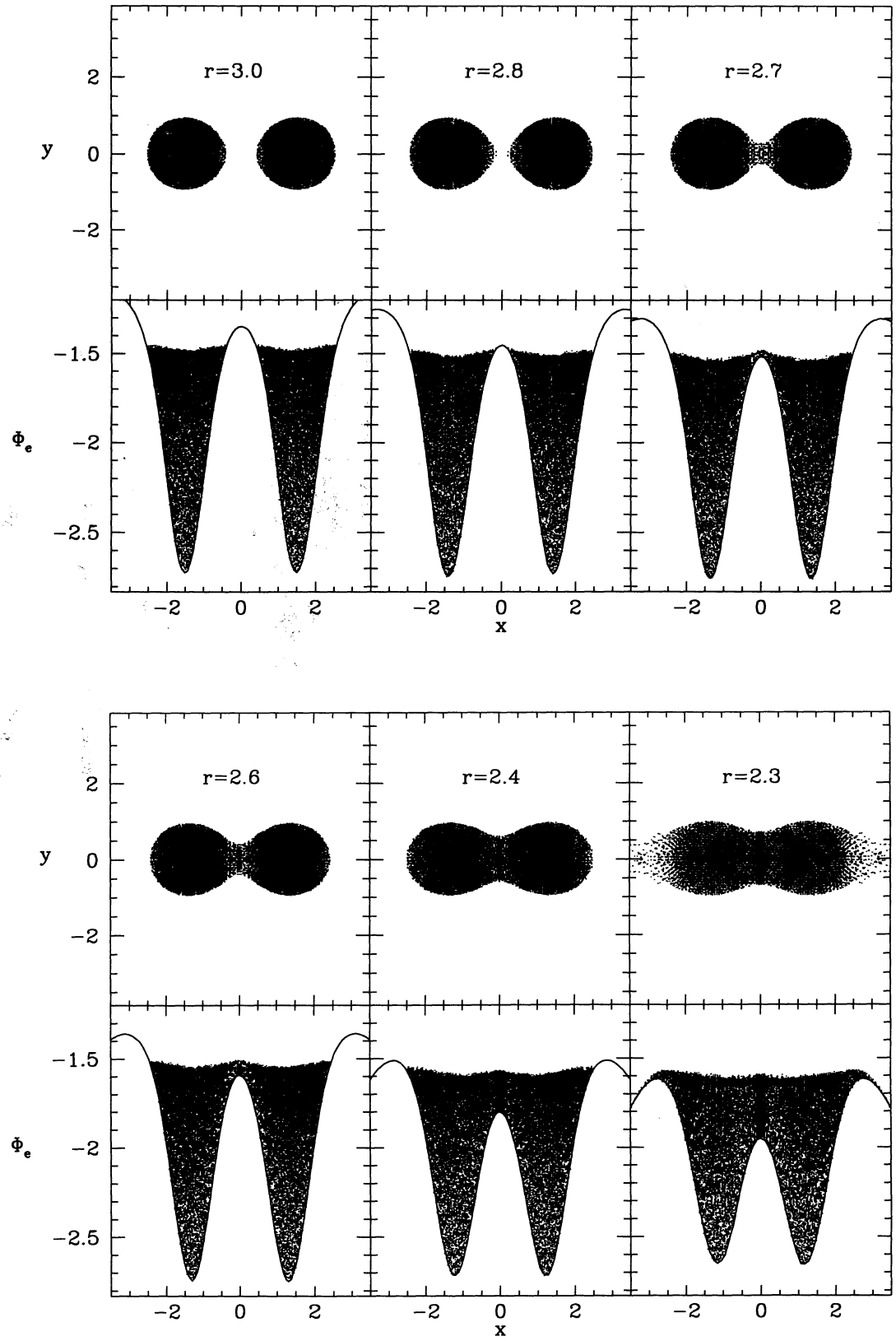

FIG. 1.—Sequence of binary equilibrium configurations for two identical polytropes with $\Gamma = 5/3$. Projections of all SPH particles onto the orbital plane are shown in the upper portion of the figure. Projections onto the (x, Φ_e) plane, where x is the coordinate along the binary axis and Φ_e is the effective potential (eq. [6]), are shown at the bottom. The solid lines show the variation of $\Phi_e(x, y = 0, z = 0)$ along the binary axis. Units are such that $G = M = R = 1$ as defined in § 2. Contact configurations are obtained when the binary separation $r \lesssim 2.8$. For $r \lesssim 2.4$, mass shedding through the outer Lagrangian points occurs, and no equilibrium configuration exists.

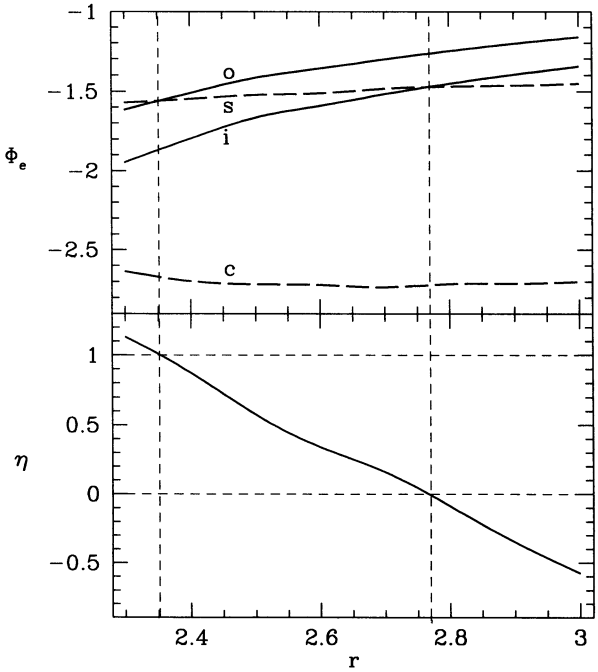

FIG. 2.—Variation of the critical potentials along the equilibrium sequence shown in Fig. 1. Values of the effective potential Φ_e at the outer Lagrangian points (o), the inner Lagrangian point (i), the fluid surface (s), and at the center of each star (c) are shown as a function of binary separation (*above*). The degree of contact η (eq. [7]) is shown below. The dashed lines show the positions of the first contact configuration ($\eta = 0$) and the Roche limit ($\eta = 1$).

Borrowing the terminology from models of W UMa binaries (Rucinski 1992 and references therein), we define the degree of contact η as

$$\eta \equiv \frac{\Phi_e^{(s)} - \Phi_e^{(i)}}{\Phi_e^{(o)} - \Phi_e^{(i)}} . \tag{7}$$

Clearly, we have $\eta < 0$ for detached configurations and $0 < \eta < 1$ for contact systems. The variation of the effective potential and degree of contact along the sequence is illustrated in Figure 2.

It is important to realize that this equilibrium sequence passes smoothly from detached to contact configurations as r decreases. This is in contrast to all binary equilibrium sequences where the mass ratio $q \neq 1$, which always terminate at a Roche limit before the surfaces of the two components come into contact. For a system with $q \neq 1$, this Roche limit corresponds to the onset of mass transfer through the inner Lagrangian point. For $q = 1$, however, the Roche limit, which we still define as the last equilibrium configuration along a sequence with decreasing r, corresponds to the onset of *mass shedding through the outer Lagrangian points* (see Fig. 1 for $r = 2.3$).

We can use our numerical solutions to calibrate deviations from Keplerian point-mass behavior in real, self-gravitating fluid systems. As an example, Figure 3 shows the variation of the orbital period as a function of r, compared to the Keplerian value $\Omega_K^2 = G(M + M')/r^3$. The deviation is about 1% at first contact, and about 6% near the Roche limit. The values of most other equilibrium quantities, such as the effective radius of each component or the degree of contact for a given binary separation, are affected at a comparable level. These deviations imply that standard models of contact main-sequence star binaries based on the Roche approximation and point-mass Keplerian relations can never be accurate to better than a few percent. Their accuracy becomes worse for systems in deeper contact and with lower mass, unevolved components (which have less centrally concentrated density profiles). In addition to these small quantitative changes, there are also important *qualitative* changes in the behavior of the system, which can lead to the development of global instabilities (LRS).

We determine the *secular stability limit* along the equilibrium sequence by locating the point where both the total energy $E = T + W + U$ and total angular momentum J are *minimum* (LRS). This is illustrated in Figure 4 (see also Fig. 2 in Paper I, where we show a comparison with LRS and other simpler models). Our numerical results provide the first accurate determination of this point for a close binary system. As can be seen in Figure 4, the minimum is very well defined and the separate minima in E and J coincide to high numerical accuracy. This is in accord with the general property that $dE = \Omega_{orb}\, dJ$ along any sequence of uniformly rotating fluid equilibria (Ostriker & Gunn 1969). Secular instability occurs very soon after contact along this sequence. The degree of contact η at the onset of secular instability is only about 20%. Thus *stable, long-lived equilibrium configurations can only exist in shallow contact.* This result could have important implications for the theoretical modeling of W UMa binaries (see § 5.2).

The positions and properties of various critical points along the sequence are summarized in Table 1.

3.2. *Dynamical Stability*

One of our most significant new results is that, even for a binary system containing a fluid as compressible as $\Gamma = 5/3$, *dynamical instabilities can still occur.* This is somewhat of a

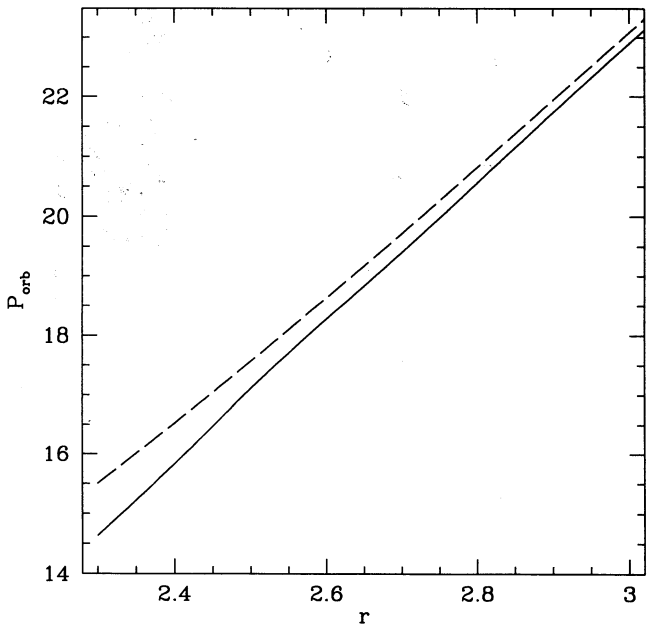

FIG. 3.—Variation of the orbital period (in the units of eq. [1]) along the equilibrium sequence shown in Fig. 1. The dashed line shows the value of the Keplerian orbital period for two point masses with the same separation r. The strong tidal interaction between the two stars makes the effective interaction potential stronger than $1/r$ and shortens the rotation period compared to a point-mass system.

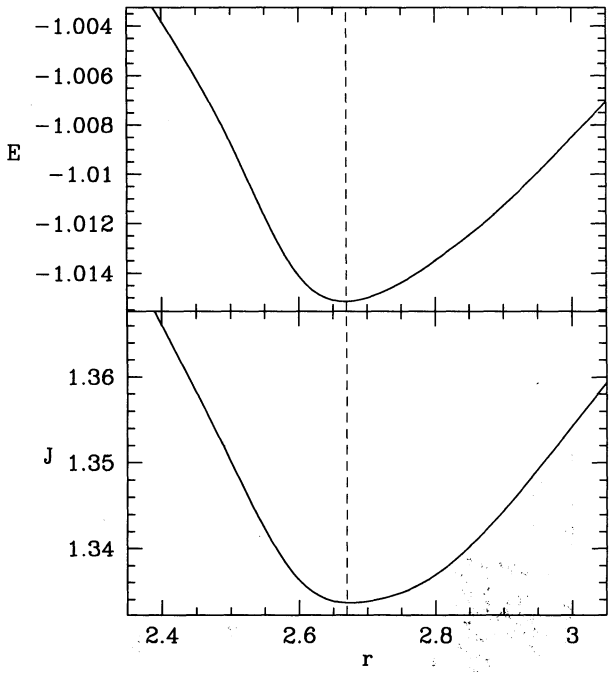

FIG. 4.—Variation of the total energy and angular momentum along the equilibrium sequence shown in Fig. 1. The vertical dashed line shows the position of the secular stability limit, where both E and J are minimum.

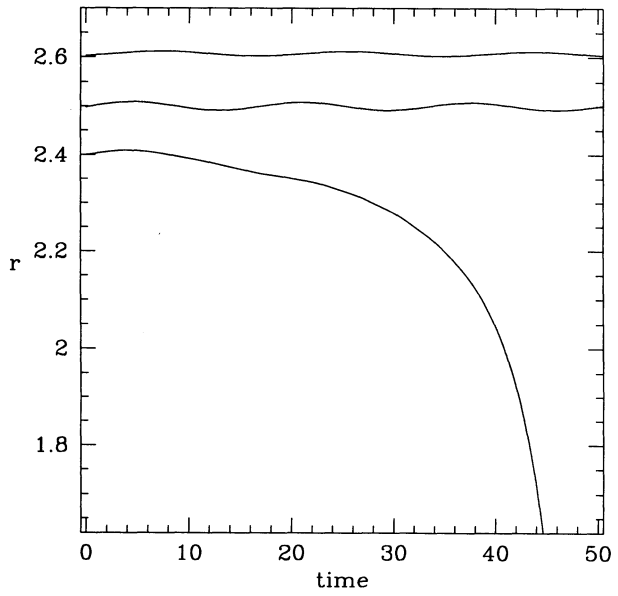

FIG. 5.—Time evolution of the binary separation r computed from dynamical calculations starting from several of the equilibrium models shown in Fig. 1. Equilibrium configurations with $r \lesssim 2.45$ are dynamically unstable.

surprise, since the results of LRS suggest that dynamical instabilities of close binary equilibrium configurations can occur only for fairly stiff equations of state, with $\Gamma \gtrsim 2$ (see LRS1, § 10 and Table 13; LRS3). However, the method of LRS applies only to *detached* systems (since the two compressible ellipsoids used to model the stars cannot overlap), whereas the dynamical instability found here for $\Gamma = 5/3$ corresponds to a configuration in deep contact, around $r = 2.4$ in Figure 1. Since tidal effects are even stronger in contact systems than in close but detached systems, it is reasonable to find that contact systems are even more susceptible to global instabilities.

As in Paper I, we determine the dynamical stability of our equilibrium solutions by using each of them as an initial condition for fully dynamical SPH integrations. Unstable systems evolve to rapid coalescence in just a few orbital periods. The results of such integrations for three of the equilibrium solutions described in § 3.1 are illustrated in Figure 5, where we show the time evolution of the binary separation. The dynamical stability limit is clearly identified at $r \approx 2.45$, corresponding to a degree of contact $\eta \approx 0.7$. Each dynamical integration, using $N \approx 20000$ SPH particles per star, took about 20 CPU hours per orbital period on the Cornell IBM ES-9000 supercomputer.

TABLE 1

CRITICAL POINTS ALONG THE EQUILIBRIUM SEQUENCE FOR TWO IDENTICAL STARS[a]

	PROPERTY				
CRITICAL POINT	r	η	P_{orb}	E	J
First Contact	2.77	0.	20.2	−1.0142	1.335
Secular Instability.....	2.67	0.22	19.0	−1.0153	1.333
Dynamical Instability.....	2.45	0.7	16.5	−1.0062	1.358
Roche Limit[b]	2.35	1.	15.2	−1.0013	1.374

[a] Units are defined in § 2.2; r is the binary separation, η is the degree of contact (eq. [7]), P_{orb} is the orbital period, and E and J are the total equilibrium energy and angular momentum.

[b] Defined as the equilibrium configuration with the minimum binary separation.

The evolution of the dynamically unstable system with $r = 2.4$ is illustrated in Figure 6. Contours of constant density in the orbital plane and perpendicular sections are shown at various times. As before, we use units such that $G = M = R = 1$, where M and R are the mass and radius of one unperturbed star. For two main-sequence stars of mass $M \approx 0.5\ M_\odot$ and unperturbed radius $R \approx 0.5\ R_\odot$, the initial binary separation is $r \approx 8 \times 10^{10}$ cm and the initial orbital period $P_{orb} \approx 3.5$ hr. The entire evolution shown in Figure 6 then takes about one day. For two white dwarfs of mass $M \approx 1\ M_\odot$ and radius $R \approx 10^{-2}\ R_\odot$, the initial binary separation is $r \approx 2 \times 10^9$ cm, the initial period $P_{orb} \approx 25$ s, and the coalescence is completed in about 2 minutes.

We can distinguish three stages in the development of the instability. In the linear stage, which lasts about one orbital period ($t = 0$ to $t \approx 20$), the separation between the two components decreases steadily and the system remains close to hydrostatic equilibrium. In the corotating frame of the binary, the relative radial velocity remains very subsonic, and the evolution remains therefore adiabatic. When the separation has decreased below $r \approx 2.3$, quasi-hydrostatic configurations no longer exist (cf. Figs. 1 and 2), and mass shedding sets in rather abruptly: matter near the outer Lagrangian points is ejected in a spiralling outflow ($t \approx 40$–50). The evolution is still adiabatic at this stage. In the final stage, the spiral arms widen and merge together ($t \approx 50$–90). The relative radial velocities of neighboring arms are now supersonic, leading to some shock heating and dissipation. As a result, a nearly axisymmetric, rapidly rotating halo forms around the central merged core. Essentially all of the gas in the halo remains bound to the core (the mass loss fraction is $< 10^{-3}$). Throughout its evolution, the system is never far from virial equilibrium (Fig. 7). This is in complete contrast to the case of a stellar collision (see, e.g., Lai,

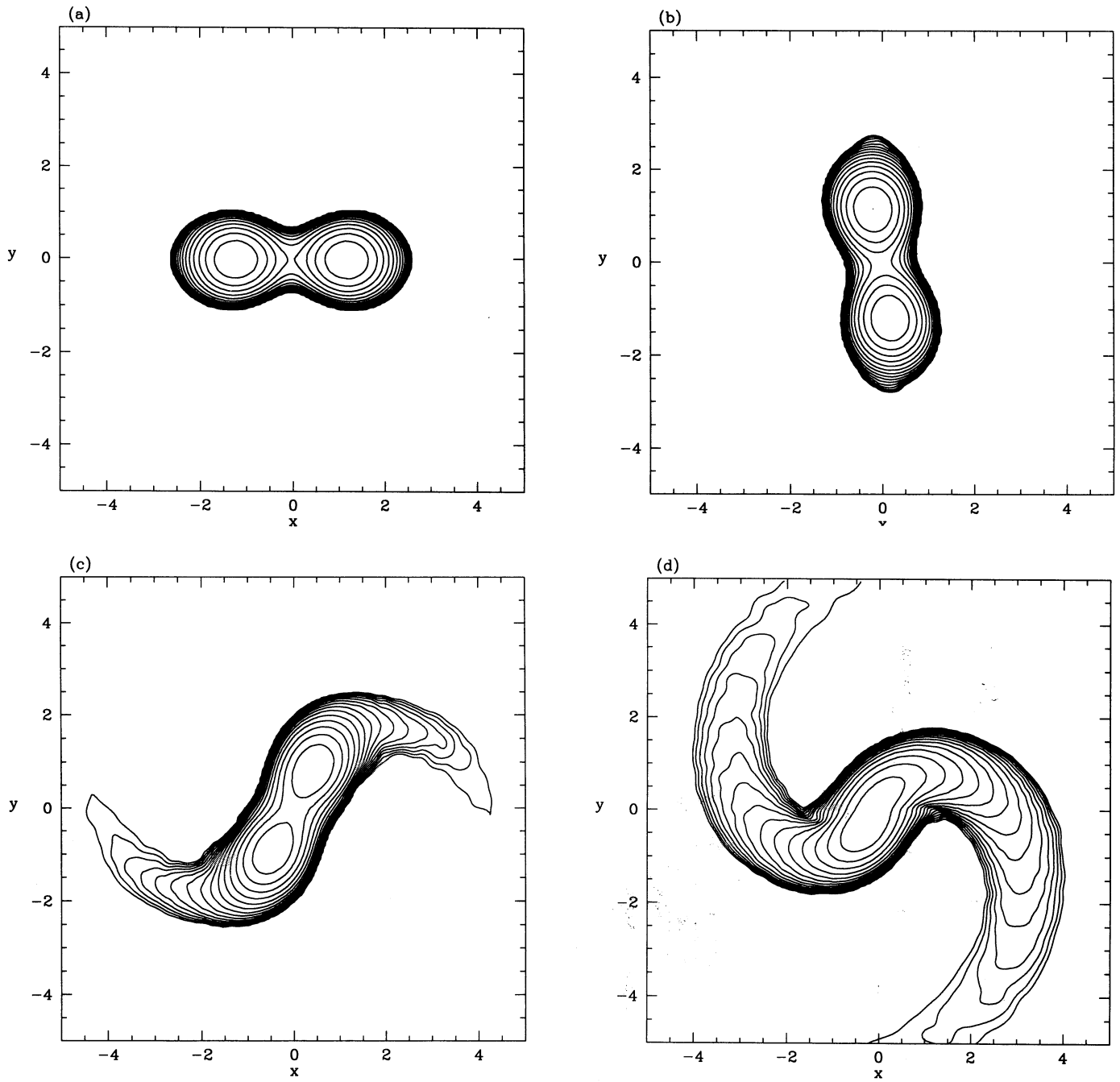

FIG. 6.—Evolution of the unstable binary with $r = 2.4$ shown in Figs. 1 and 5. Contours of equal density in the orbital plane are shown as a function of time: (*a*) $t = 0$; (*b*) $t = 20$; (*c*) $t = 40$; (*d*) $t = 45$; (*e*) $t = 45$; (*f*) $t = 50$; (*g*) $t = 60$; (*h*) $t = 70$; (*i*) $t = 90$; and (*j*) $t = 90$. The scale is logarithmic, with 16 contours covering 4 decades down from the value $\rho_{max} \simeq 1.5$ in the unit of eq. [3]. The orbital rotation is counterclockwise. Vertical sections are shown in (*e*) and (*j*). All other plots show sections through the orbital plane.

Rasio, & Shapiro 1993c), where a large initial excess of kinetic energy has to be converted into other forms.

The internal structure of the final merged configuration is similar to that obtained and described in detail by RS for two identical polytropes with $\Gamma = 2$. About 80% of the total mass is contained inside a uniformly rotating core where the density $\rho/\rho_c \gtrsim 0.1$. The rotation inside this core is nearly maximal, with $\Omega \simeq 0.5$ in our units. About 20% of the mass is contained in an extended halo (outer radius $R_h \gtrsim 20\ R$ in the equatorial plane) of shock-heated gas in differential rotation. The structure of the halo is pseudobarotropic with angular velocity $\Omega \propto r_{cyl}^{-\nu}$, where $r_{cyl} = (x^2 + y^2)^{1/2}$ and $\nu \lesssim 2$.

The ratio $T/|W|$ of kinetic energy of rotation to gravitational binding energy (Fig. 7) is <0.14 at the end of the coalescence, consistent with the axisymmetric shape (see, e.g., Tassoul 1978). However, the final value, $T/|W| \approx 0.12$, is considerably higher than the maximum value for stability against mass shedding allowed for a *uniformly rotating* axisymmetric polytrope, $(T/|W|)_{max} \approx 0.06$ (see Table 3 of LRS1). This is simply because differential rotation is very important in the

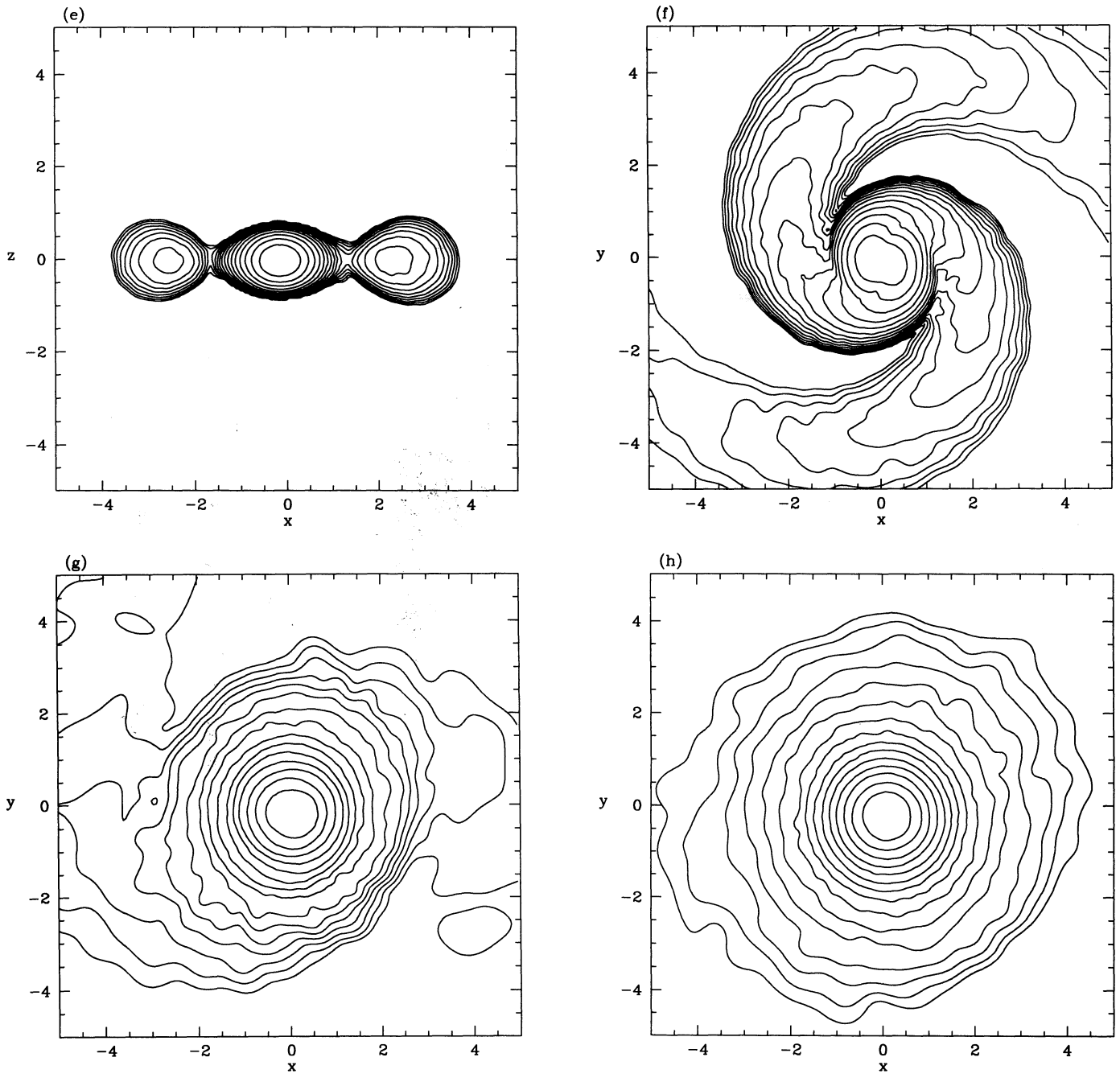

FIG. 6—*Continued*

halo. Indeed, it is generally found that relaxing the assumption of uniform rotation allows compressible equilibria with considerably higher values of $T/|W|$ to exist (see Bodenheimer & Ostriker 1973).

4. BINARIES WITH TWO UNEQUAL MASSES

Equilibrium sequences with decreasing r for two nonidentical stars terminate at a Roche limit corresponding to a *semi-detached* configuration. Which star fills its critical lobe first depends on the mass-radius relation for the two components. As discussed in § 2, we consider two simple cases here. For binaries containing two degenerate stars we set $K = K'$, which leads to the relation $(R/R') = (M/M')^{-1/3}$. To model systems containing two low-mass main-sequence stars, we assume $R/R' = M/M'$.

4.1. *Low-Mass Main-Sequence Stars*

With a mass-radius relation of the type $R/R' = M/M'$, the more massive component (primary) is also the larger in size, and it has the smaller mean density of the two. At the Roche limit, it is therefore the primary that fills its critical lobe in the effective potential. This is illustrated in Figure 8, where we show three configurations with mass ratio $q = 0.5$ near the Roche limit. These configurations were constructed using the

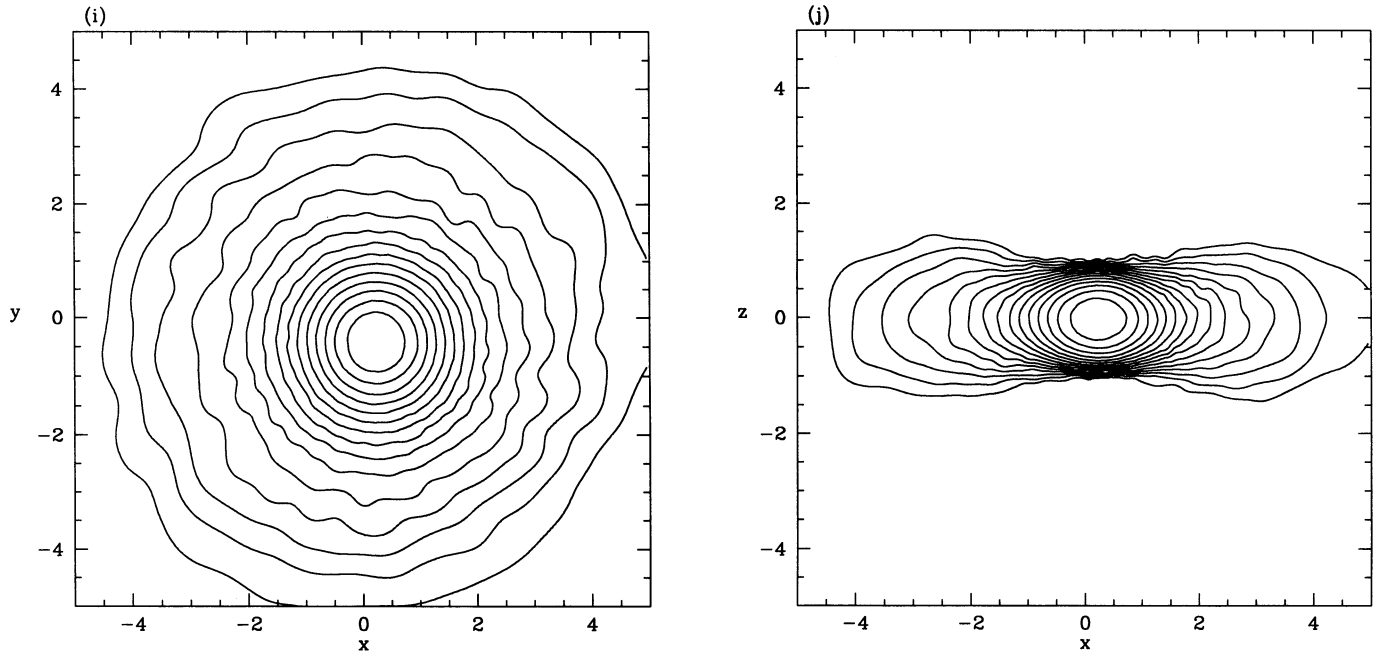

FIG. 6—*Continued*

quasi-static scanning technique described in § 2.3 of Paper I. The minimum (Roche limit) separation $r_{\rm lim} \approx 2.30$–2.33 is very well determined numerically (to better than 1%). Binary equilibrium configurations with $r < r_{\rm lim}$ do not exist.

If one were to continue decreasing r quasi-statically below $r_{\rm lim}$, material from the primary would flow onto the surface of the secondary (see Fig. 8 for $r = 2.27$). This is a possible way of continuing the equilibrium sequence beyond the Roche limit. Unfortunately, the mass ratio is changed during this process, becoming closer to unity, and the structure of the secondary is no longer that of a polytrope. Since the specific entropy is lower in the primary, the transferred material is buoyant and remains stably on top of the lower entropy material in the original secondary. Eventually, when the secondary fills its critical lobe, a contact configuration is obtained, with an interior structure of the type considered in the contact discontinuity model of Shu, Lubow, & Anderson (1976). In reality, however, *dynamical* (as opposed to quasi-static) mass transfer would lead to shock heating of the material as it hits the surface of the secondary (see below), and the specific entropy in the common envelope could be considerably higher. We do not discuss further contact systems with $q \neq 1$ in this paper, focusing instead on the properties of semidetached configurations.

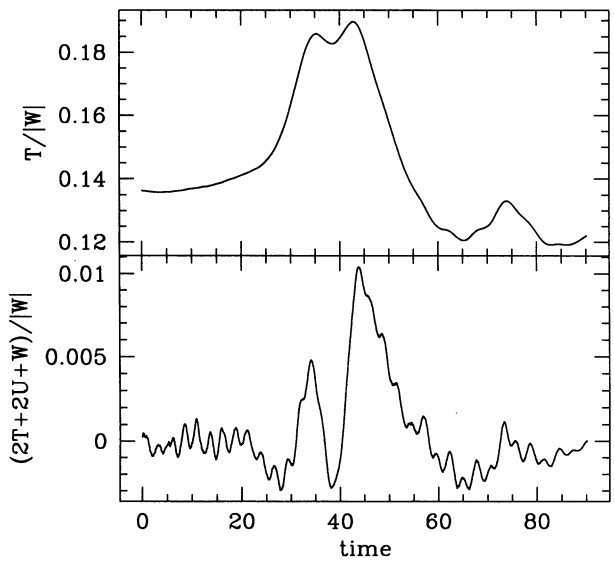

FIG. 7.—Evolution of the virial ratio $(2T + 2U + W)/|W|$ (cf. eq. [4]) and the ratio $T/|W|$ of kinetic energy of rotation to gravitational binding energy during the dynamical coalescence shown in Fig. 6.

Using SPH, we have constructed several equilibrium sequences for decreasing values of the mass ratio. In each case we determine the secular stability of the Roche limit configuration by following the variation of the total angular momentum J along the sequence.[5] The results are shown in Figure 9. We see that *there exists a critical value of the mass ratio* $q_{\rm crit} \approx 0.4$ *where the Roche limit configuration becomes secularly unstable.* For $q < q_{\rm crit}$, there exists an *unstable branch* of configurations between the minimum of J and the Roche limit. Possible implications of these results for W UMa binaries are discussed in § 5.1 below.

Figure 9 shows a comparison of our SPH results with those obtained in LRS4 using a semianalytic variational method. In all cases, the equilibrium $J(r)$ curves determined by the two methods are in excellent quantitative agreement (to within a few parts in 10^3) up to the Roche limit as determined by SPH. However, the method of LRS cannot provide the *location* of the Roche limit to better than about 20% in r. A similar situation was encountered in LRS1 (cf. § 3 of that paper) with respect to the mass-shedding limit along equilibrium sequences of isolated, rapidly rotating stars. The variational method of LRS can be used to determine equilibrium properties of uni-

[5] Total energy can be considered also, and leads to the same conclusions. However, by comparing our results to those of LRS for large r, we find that our numerical accuracy in the calculated value of J is generally better.

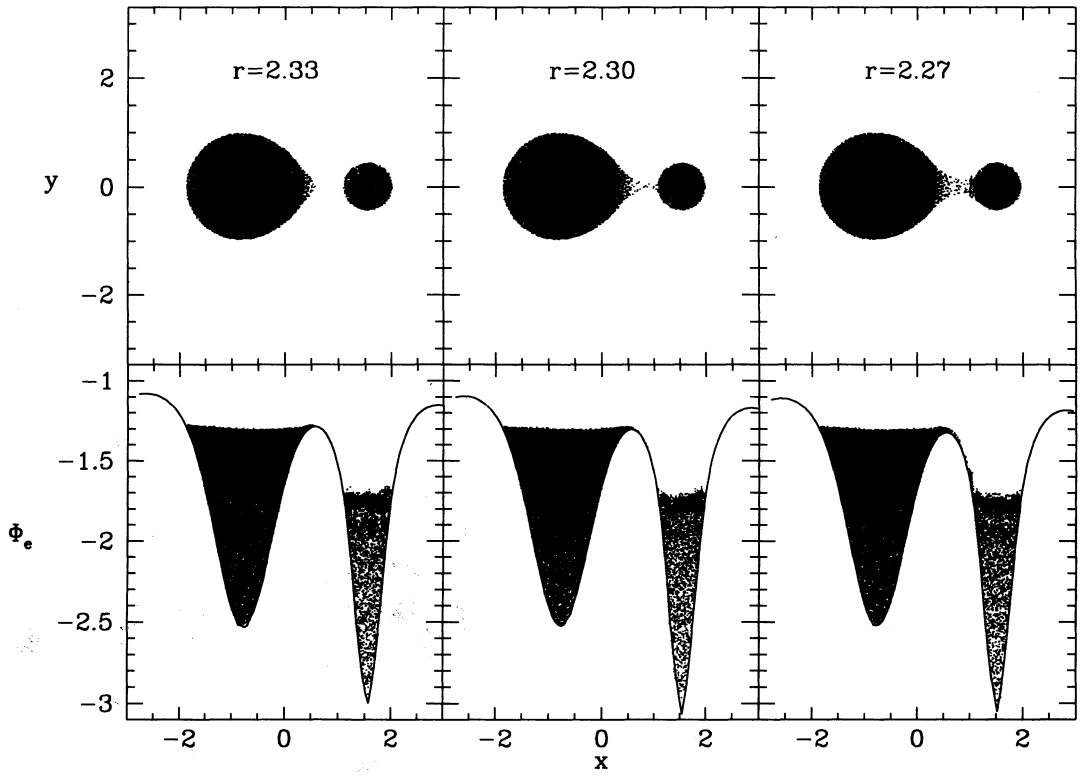

FIG. 8.—Equilibrium configurations near the Roche limit for a binary containing two low-mass main-sequence stars with mass ratio $q = 0.5$. Conventions are as in Fig. 1. The more massive (less dense) star is on the left. The Roche limit is clearly identified at a binary separation $r = r_{\rm lim} \approx 2.30$–$2.33$.

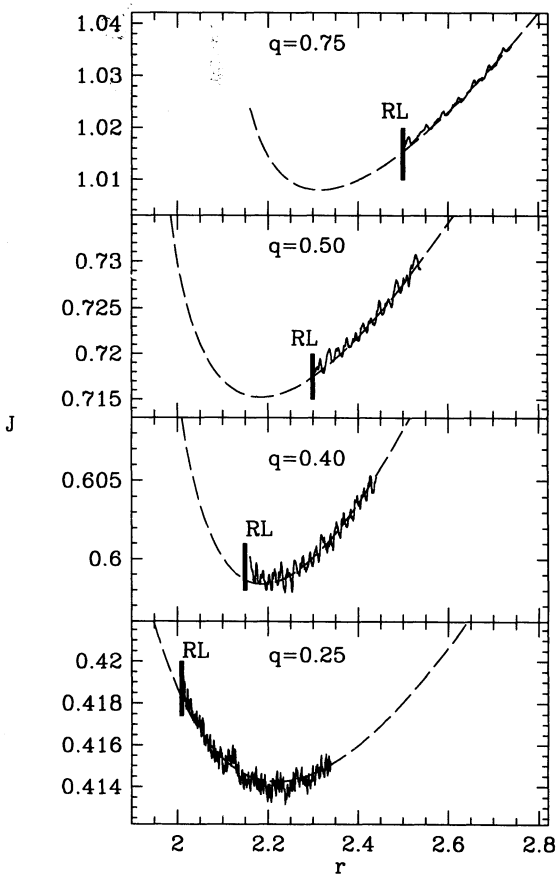

formly rotating polytropes quite accurately up to the mass-shedding limit, but it cannot by itself predict accurately the position of the mass-shedding limit.

Noting that the Roche limit configuration for $q = 0.25$ is located far beyond the secular stability limit along the sequence, we decided to test its *dynamical* stability. Recall that the onset of dynamical instability always occurs further along the sequence (at smaller r) than the secular stability limit. However, secularly unstable configurations may remain dynamically stable all the way to the Roche limit (see LRS4, § 3.3). For polytropes with $n = 1.5$ and $R/R' = M/M'$, Figure 4 of LRS4 does in fact predict that configurations with sufficiently small mass ratio should become dynamically unstable.

The results of several dynamical SPH integrations for binaries with $q = 0.25$ are illustrated in Figure 10. There is indeed a dynamical instability developing just before the Roche limit along the equilibrium sequence, at $r = r_{\rm dyn} \approx 2.05$–$2.1 > r_{\rm lim} \approx 2.01$–$2.03$. For an initial configuration with $r = 2.05$, we find that the orbit decays rapidly, leading almost immediately to the onset of dynamical mass transfer onto the small secondary (Fig. 10*c*). Numerical integrations starting from $r = 2.1$ and $r = 2.2$ were also performed and showed only small epicyclic oscillations (as in Fig. 5), with no sign of coalescence. Thus the dynamical stability limit for the sequence

FIG. 9.—Variation of the total angular momentum J as a function of binary separation r along several equilibrium sequences for two low-mass main-sequence stars. The solid lines show our numerical results, terminating at the Roche limit configuration along each sequence (indicated by a solid vertical segment). The dashed lines are from the semianalytic calculations of LRS4. When the mass ratio $q \lesssim 0.4$, there exists a branch of secularly unstable configurations between the minimum of J and the Roche limit.

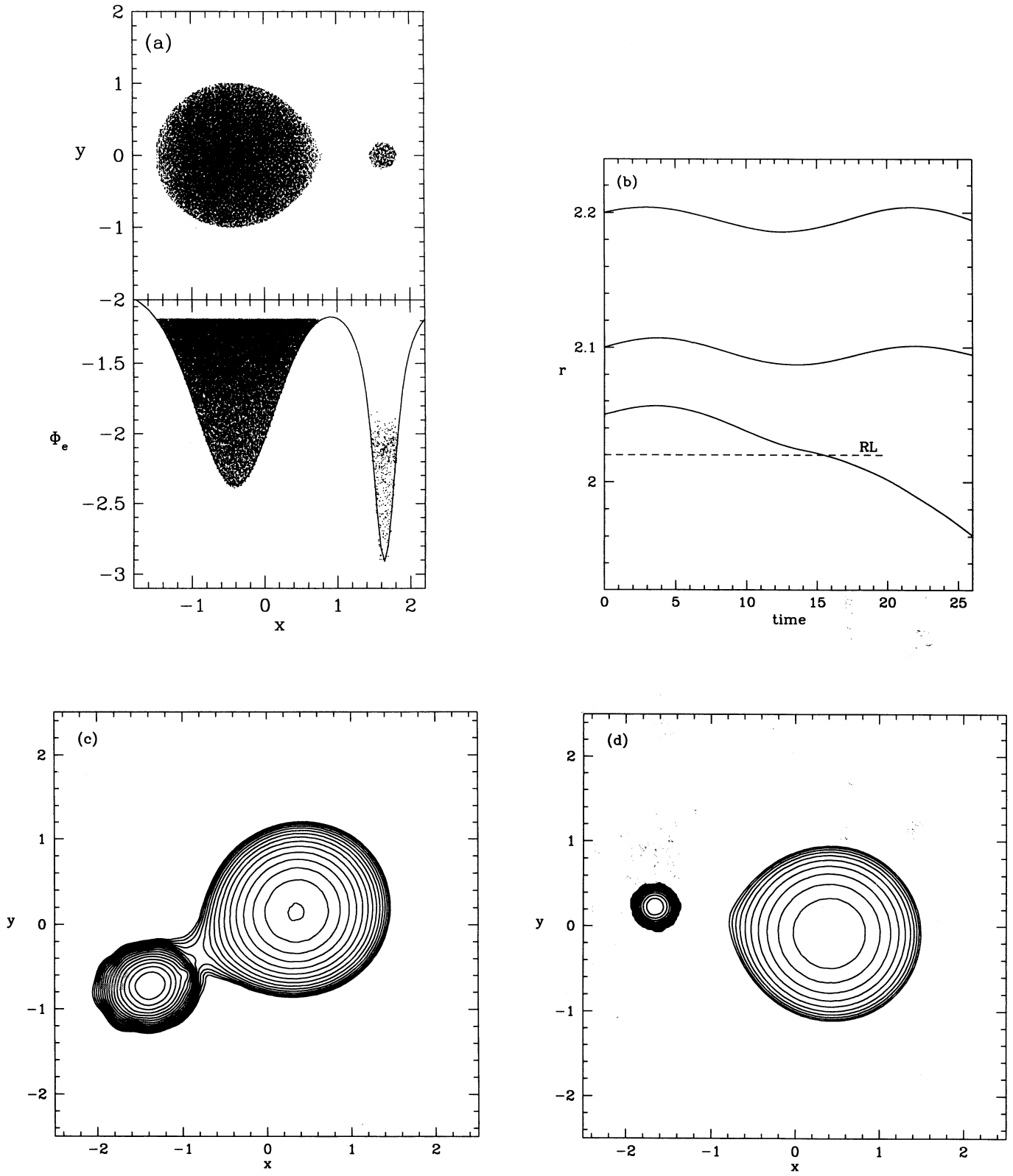

FIG. 10.—Dynamical evolution of a system containing two low-mass main-sequence stars with mass ratio $q = 0.25$. In (*a*), we show the equilibrium configuration with $r = 2.05$, just below the Roche limit; conventions are as in Figs. 1 and 8. The more massive but less dense star (primary) is on the left. In (*b*), we show the dynamical evolution of the separation r for systems with three different initial separations: the system with $r = 2.05$, shown in (*a*), is clearly unstable, while those with $r = 2.1$ and $r = 2.2$ are stable. The horizontal dashed line marks the position of the Roche limit (onset of mass transfer). In (*c*) we show how the unstable binary with $r = 2.05$ has evolved when $t = 25$. For comparison, in (*d*), we also show the stable system with $r = 2.1$ at the same time $t = 25$. In (*c*) and (*d*), conventions are as in Fig. 6.

with $q = 0.25$ is at $r_{dyn} \approx 2.05$–2.1. Sequences with even smaller values of q may be susceptible to the same dynamical instability well before reaching the Roche limit. However, we caution that the interpretation of our numerical results for this case is complicated by the highly unstable mass transfer following Roche lobe overflow. Indeed, the mass transfer is from the more massive to the less massive component, implying a tendency for the separation to decrease during mass transfer, in addition to the adiabatic increase in radius of the mass-losing star (see, e.g., Shore, Livio, & van den Heuvel 1994). Since the numerically determined dynamical stability limit is so close to the Roche limit, we cannot strictly rule out the possibility that the instability we see developing is in fact driven mostly, or even entirely, by the unstable response of the system to the mass transfer.[6] Since our simple models for main-sequence stars can apply only to a fairly small range of masses, $0.1 \lesssim M/M_\odot \lesssim 0.5$, the question of what really happens to these models for extreme mass ratios is obviously of limited astrophysical interest.

[6] The statement made in § 5 of LRS4 that all sequences with $0.25 \leq p < 1$ are dynamically stable may therefore be correct. However, it should have read $0.25 < p < 1$. (The mass ratio is denoted by p in LRS).

4.2. *Degenerate Configurations*

For degenerate systems with $q \neq 1$, the more massive (and denser) component typically suffers very little tidal deformation compared to the other, less massive component (cf. LRS4, § 4.4). As a result, the overall destabilizing effect of tidal interactions in the binary system is greatly reduced. Using SPH to construct equilibrium sequences, we find that, for all mass ratios, *close binaries containing two degenerate stars remain secularly (and, therefore, dynamically) stable all the way to the Roche limit.* An example is shown in Figure 11 for $q = 0.5$. The equilibrium configuration with $r = 3.9$ is very close to the Roche limit, and its angular momentum is still well above the minimum value $J_{min} \simeq 0.86$ calculated using the method of LRS4.

Stability of all hydrostatic equilibrium configurations does not say anything about how the system will respond to mass transfer after the loss of angular momentum drives it beyond the Roche limit. Since the mass-losing component responds adiabatically by expanding in size, one may expect the mass transfer itself to be dynamically unstable. Unless the orbit can expand sufficiently to counteract the tendency of the mass-losing star to overflow its Roche lobe even more, the mass-transfer rate will grow catastrophically (Shore et al. 1994).

We demonstrate this instability of the mass transfer itself by studying the dynamical evolution of the (stable) equilibrium configuration shown in Figure 11*a*. This configuration is as close to the Roche limit as we could realize numerically, with just a few SPH particles having crossed the inner Lagrangian point. The initial separation is $r = 3.90$ and the corresponding orbital period is $P_{orb} \approx 39$ in our units. The evolution is shown in Figures 12 and 13. We see that the mass transfer is indeed unstable, with the mass transfer rate increasing on a timescale

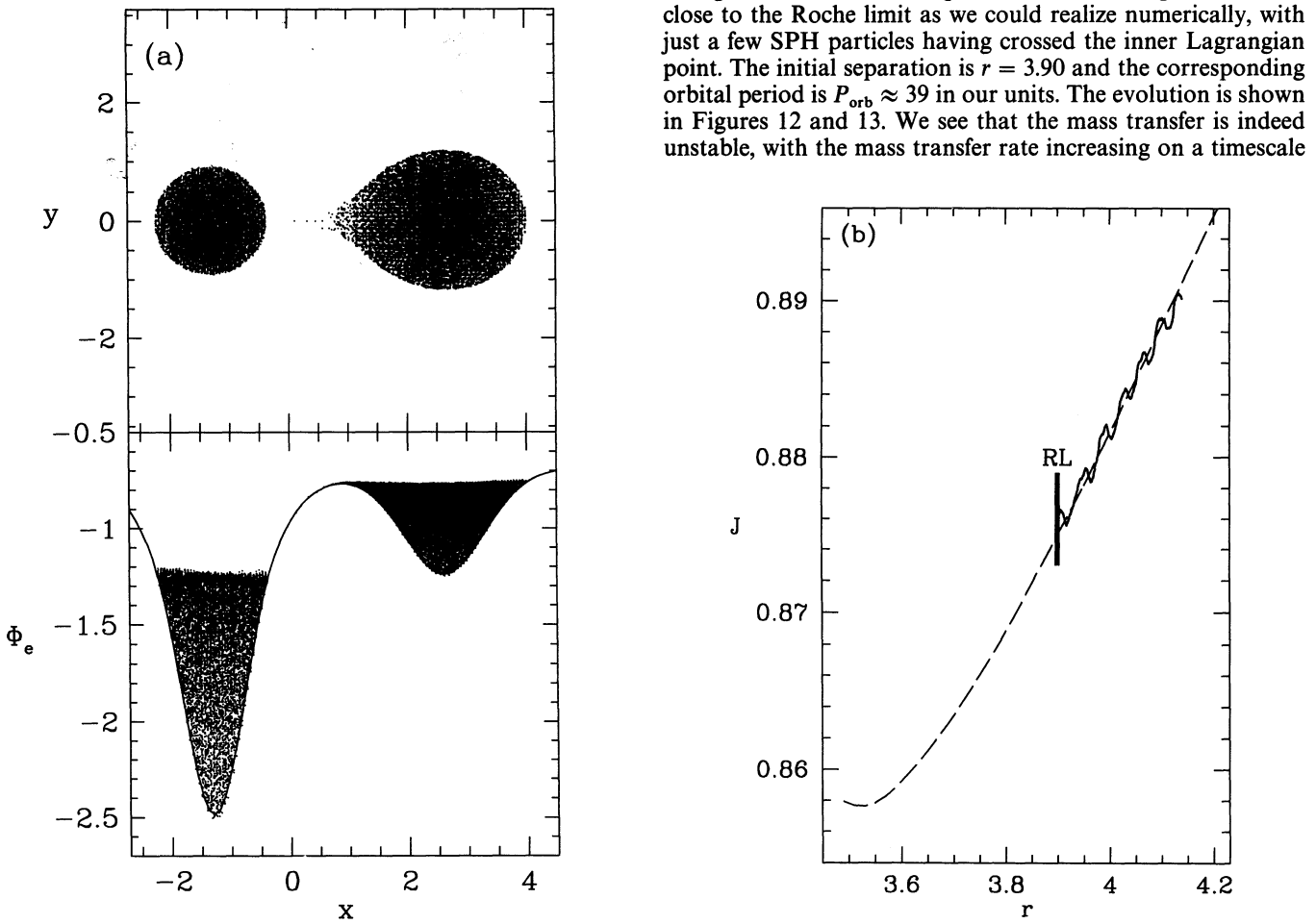

FIG. 11.—Roche limit configuration for a system containing two low-mass white dwarfs with $q = 0.5$. In (*a*), conventions are as in Figs. 1 and 8. The lower mass (and lower density) star is on the right, about to start mass transfer onto the higher mass star on the left. In (*b*), conventions are as in Fig. 9.

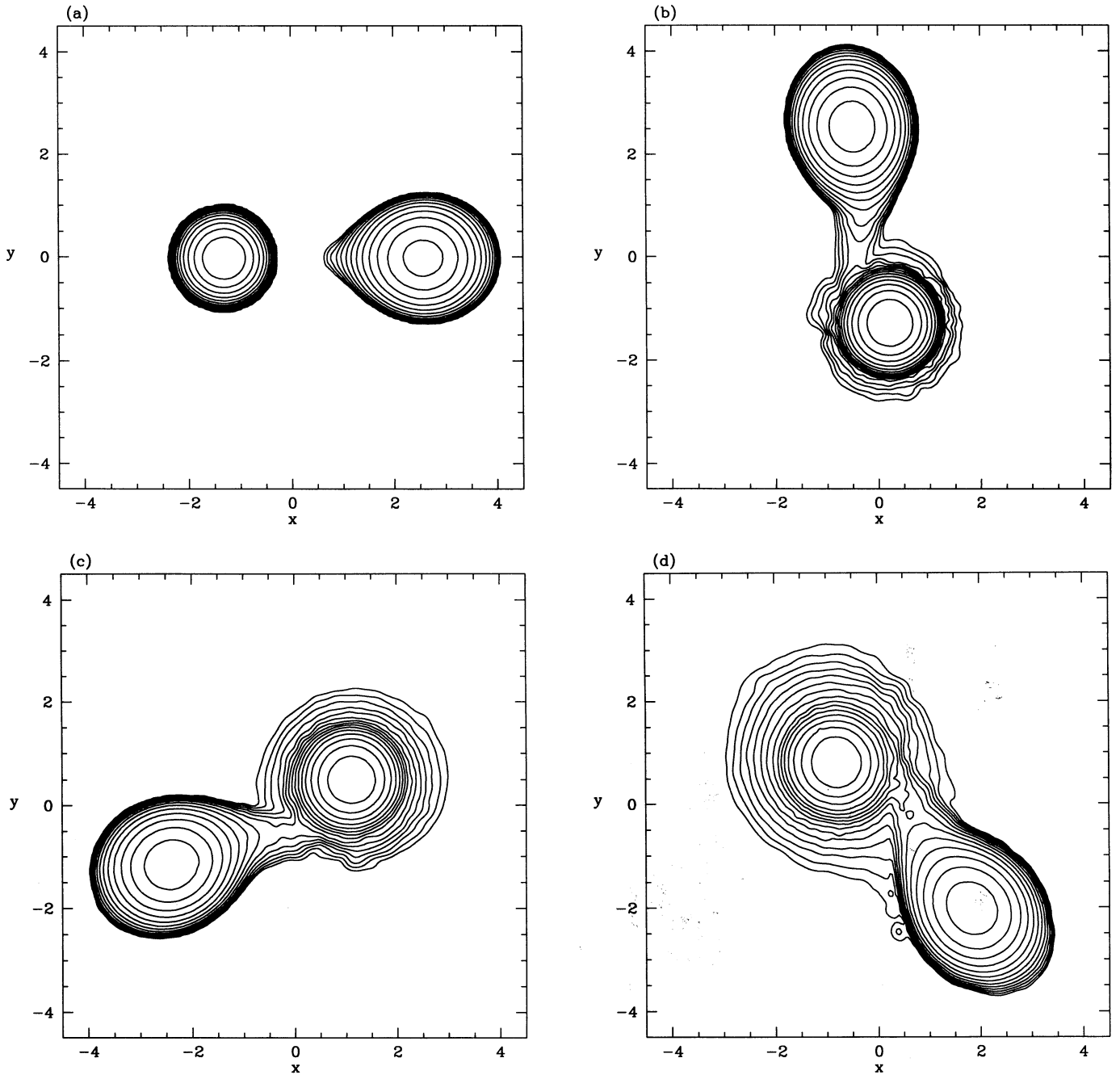

FIG. 12.—Dynamical evolution of a system containing two low-mass white dwarfs with $q = 0.5$: (*a*) $t = 0$; (*b*) $t = 50$; (*c*) $t = 100$; (*d*) $t = 150$; (*e*) $t = 200$; (*f*) = 220; (*g*) $t = 250$; and (*h*) $t = 250$. The initial binary separation is $r = 3.9$, just beyond the Roche limit. Although all equilibrium configurations down to the Roche limit are stable, the mass transfer itself is dynamically unstable, leading to the complete coalescence of the binary in about five orbital periods ($P_{orb} \approx 39$ at $t = 0$). Conventions are as in Fig. 6.

comparable to the orbital period. As before (cf. Figs. 5 and 10*b*), we have checked the stability of systems with slightly larger separation, $r = 4.0$ and $r = 4.1$, by calculating their dynamical evolution for several orbital periods, and found no sign of instability. The mass transfer rate increases very slowly at first, with the secondary's mass loss being only 10% after about four complete orbital periods (Fig. 13*a*), but then accelerates rather abruptly. Complete tidal disruption of the secondary is observed after about five orbital periods. (Figs. 12*e*–12*g*). The final configuration is again an axisymmetric merger with a core-halo structure, the core containing the primary and the halo being made of shock-heated material from the disrupted secondary. Note the pronounced cusp in the isodensity contours near the equatorial plane (Fig. 12*h*), indicating a maximal rotation rate. To construct Figure 13, we have determined the structure of the "instantaneous" effective potential (eq. [6]) at every time during the evolution. This requires iterations, since the instantaneous value of Ω_{orb} is determined from the motion of the fluid contained inside the (inner) critical potential lobe. The orbital angular momentum

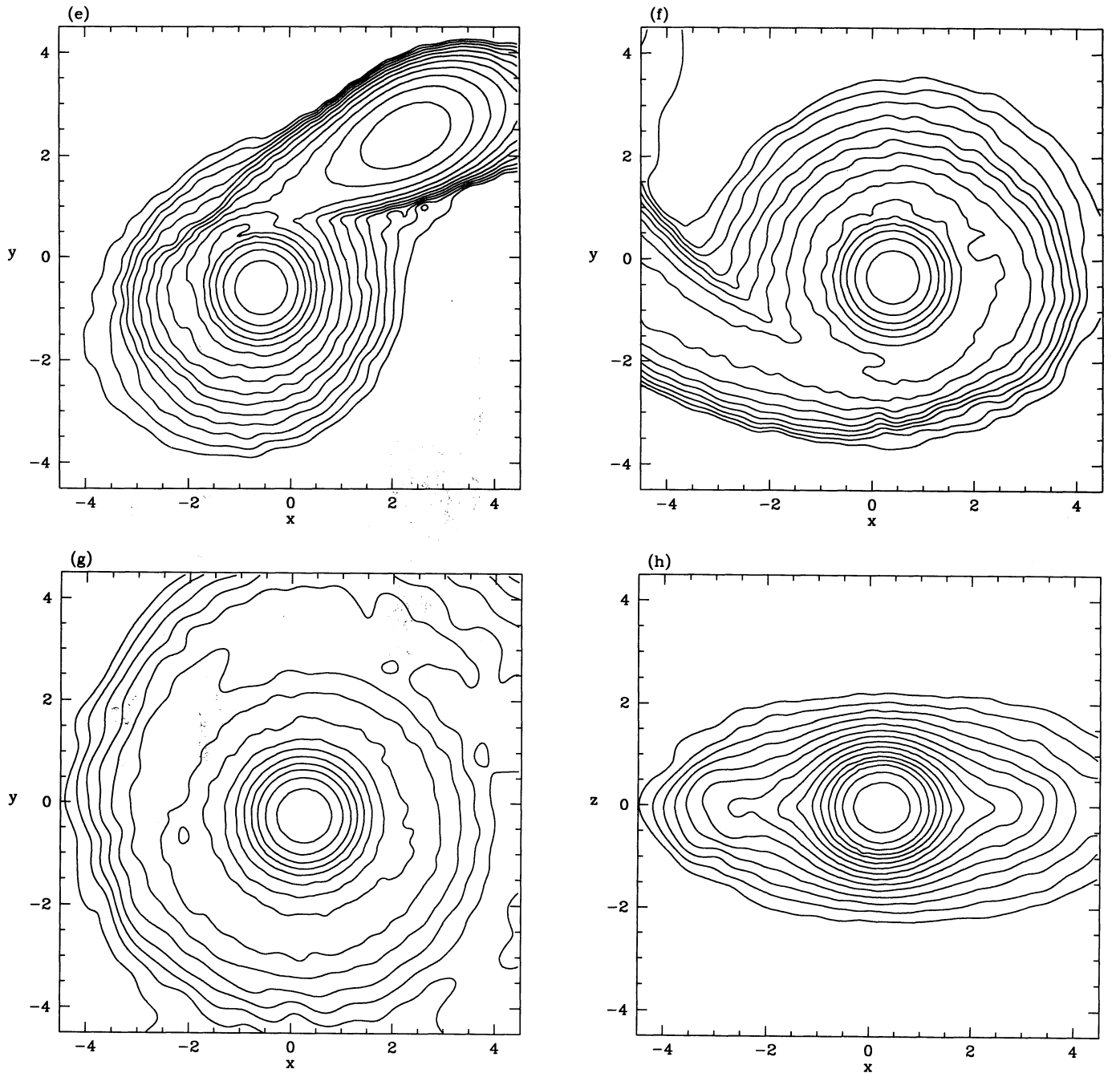

FIG. 12—*Continued*

J_{orb} corresponds to the center-of-mass motion of the two components. Clearly, orbital angular momentum is *lost* during mass transfer, leading to rapid orbital decay and the unstable increase in the mass transfer rate (Fig. 13*a*).

The evolution of the density and specific entropy profiles along the binary axis is illustrated in Figure 13*b*. The density inside the primary *decreases* during the evolution. This is because shock heating as the massive accretion column impacts the surface (Figs. 12*b*–12*d*) leads to a slight increase in the specific entropy throughout the interior of the primary. The material that accumulates on top of the primary's surface inside its critical potential lobe is of very low density (high entropy), and its mass is essentially negligible in determining the final structure of the core (in the absence of shock heating, the slight increase in mass of the primary would make its density *increase*). Outside of the critical lobe, rotational support is important. However, the final merged configuration has $T/|W| \approx 0.08$, far below the secular stability limit for axisymmetric configurations at $T/|W| \approx 0.14$ (see, e.g., LRS1).

As we mentioned in the Introduction, coalescing white dwarf binaries are potentially important sources of low-frequency gravitational waves. In Figure 14, we show examples of gravitational radiation waveforms emitted during the final coalescence, both for a dynamically unstable system with $q = 1$

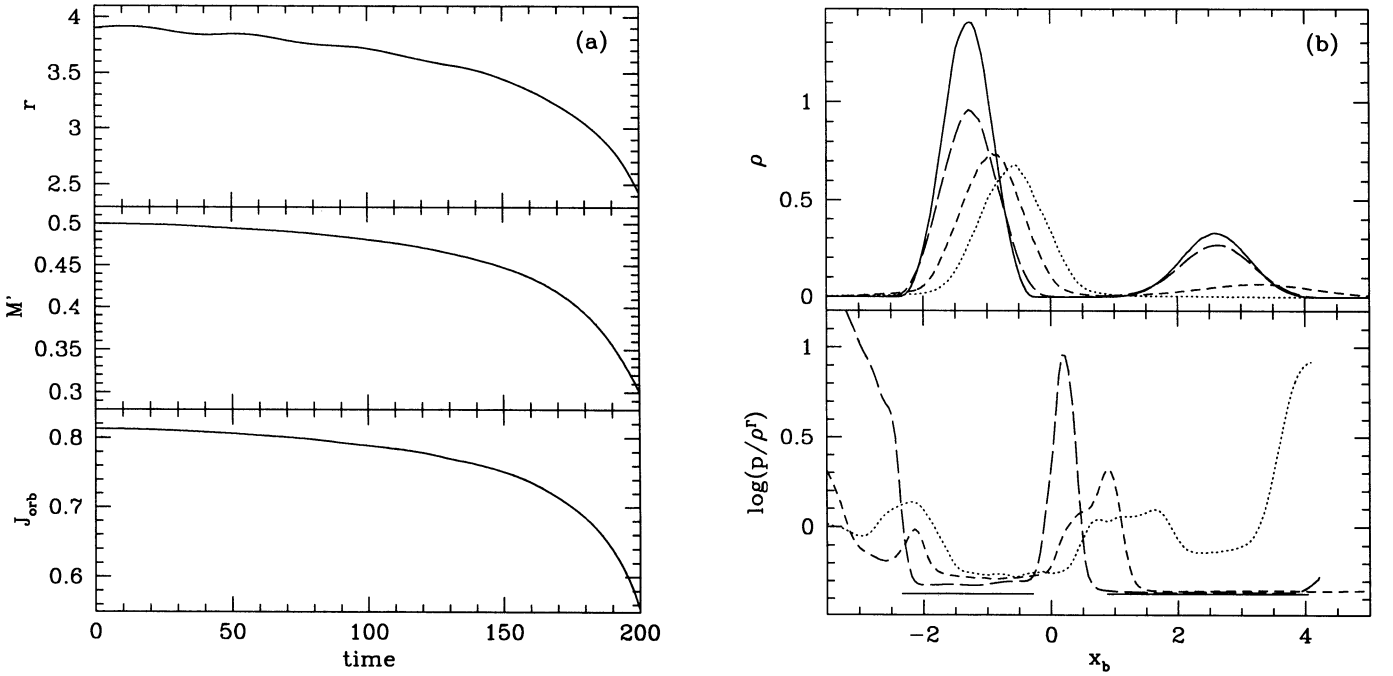

FIG. 13.—Evolution of various quantities during dynamically unstable mass transfer for the binary system shown in Fig. 12. In (*a*) we show the separation r, mass of the secondary M', and orbital angular momentum J_{orb} as a function of time. In (*b*), we show the density and specific entropy ($s \propto \log [p/\rho^{\Gamma}]$) profiles along the binary axis at $t = 0$ (*solid lines*), $t = 100$ (*long-dashed lines*), $t = 200$ (*short-dashed lines*), and $t = 220$ (*dotted lines*).

(§ 3.2), and for the system with $q = 0.5$ driven by unstable mass transfer (considered above). These were calculated as in Paper I and RS, in the quadrupole approximation. The two waveforms are strikingly different. One obvious difference in overall timescale comes from our normalization to the mass and radius of the primary. But there are also important *qualitative differences* caused by the different hydrodynamic processes at work. For the system with $q = 0.5$ driven by unstable mass transfer, the amplitude of the waves *decreases* while the frequency remains essentially constant (it actually decreases also, but very slightly). For the dynamically unstable system with $q = 1$, both the amplitude and the frequency *increase*. In both cases, however, the emission shuts off abruptly at the very end of the evolution. This is because the system evolves rapidly to a stationary axisymmetric configuration, which does not radiate gravitational waves (cf. Paper I; RS).

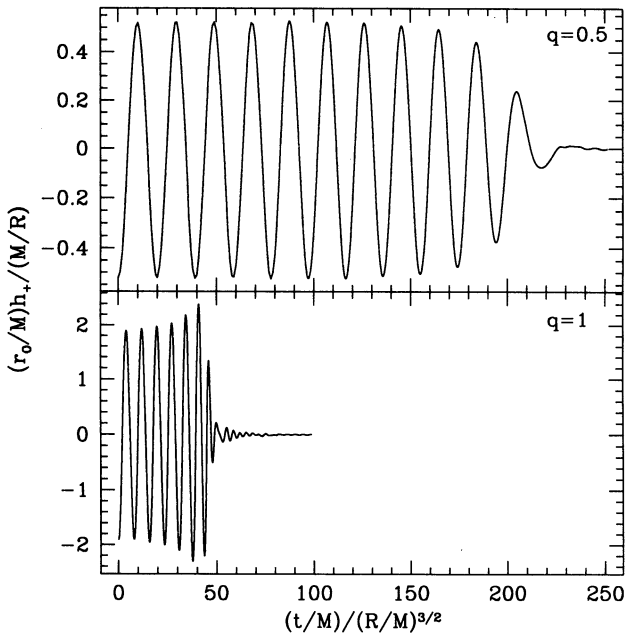

FIG. 14.—Gravitational wave amplitude h_+ as a function of retarded time for the dynamical evolution shown in Fig. 12. Here quantities are labeled in geometrized units ($G = c = 1$). The amplitude is shown for an observer situated at a distance r_o along the rotation axis. For comparison, we also show the amplitude of the waves emitted during the dynamical coalescence of a system with $q = 1$.

5. DISCUSSION

5.1. *Evolution of W Ursae Majoris Binaries*

It is tempting to envision (cf. Rasio 1993, 1994) that the secular orbital decay of a contact system through loss of angular momentum (by gravitational radiation or via magnetized winds), probably accelerated by viscous dissipation (see below), could eventually bring the two components sufficiently close together to make the system dynamically unstable. The following hydrodynamic evolution leads to the rapid coalescence of the two stars into a single, rapidly rotating object (Figs. 6*i* and 6*j*) which one could call a "proto–blue straggler."

It should be stressed, however, that hydrodynamic calculations can only reveal the new hydrostatic equilibrium configuration reached by the system following complete coalescence. This configuration is in *mechanical* equilibrium, but far from thermodynamic equilibrium. On a timescale much longer than the hydrodynamic timescale, various dissipative transport processes will be operating that can modify considerably the structure of the object. Thus the results of purely hydrodynamic calculations cannot directly predict the *observable properties* of blue stragglers. For example, angular

momentum may well be removed very efficiently from the rapidly and differentially rotating outer halo through a magnetized wind (cf. Leonard & Clement 1993). The outer layers of the observed blue straggler could then appear to be rotating slowly, even if the interior is still spinning rapidly. Thus the rapid rotation predicted by hydrodynamic calculations (which conserve angular momentum) may never be observed directly. Indeed, at least some blue stragglers are known observationally to be slow rotators (Mathys 1991).

Our results do not confirm the suggestion by Williams & Roxburgh (1976) that *all* contact systems with $q = 1$ should be dynamically unstable to mass transfer from one component to the other. This was their proposed explanation for why W UMa systems with q close to unity are not observed. It should be noted that such a system may now in fact have been found (Samec, Su, & Dewitt 1993). We have calculated the dynamical evolution of a number of contact configurations with $q = 1$ (cf. Fig. 5). We have not detected any tendency for an asymmetric unstable mode to develop, at least within a few orbital periods. Even during the evolution of a dynamically unstable system to coalescence (Fig. 6), there is no sign of an asymmetry developing. It is important to note that no assumption was made about a mirror symmetry between the two components in our calculations. Each star was modeled separately using a completely independent set of SPH particles and the gravitational field is calculated on a cartesian grid without any assumption about the geometry. In addition, our polytropic models respond adiabatically by expanding when they lose mass, since $(\delta R/\partial M)_K < 0$. This should make a binary system particularly susceptible to mass transfer instabilities. Instead, the model of a $0.6\ M_\odot$ main-sequence star considered in detail by Williams & Roxburgh (1976) has $(\partial R/\partial M)_S > 0$. Strictly speaking, however, we cannot rule out that an *overstable* asymmetric mode of oscillation may exist for all contact configurations with $q = 1$. This mode could grow in amplitude over a timescale long compared to the few orbital periods that we have followed to establish the *orbital* stability of the equilibrium solutions. Indeed, the dynamical instability of the orbit that we identified numerically in RS and analytically in LRS corresponds to a truly *unstable* (as opposed to overstable) mode of oscillation of the binary system. In the presence of this unstable mode, the separation r will never increase again once it starts decreasing (cf. Fig. 5). Thus a dynamical integration following just one complete epicyclic oscillation is in principle sufficient to establish whether a particular solution is unstable.

Our results concerning the *secular stability* of contact binaries have important implications for the interpretation of their observed characteristics. To our knowledge, secular (tidal) instabilities have never been discussed before in the context of W UMa binaries, although van't Veer (1979) correctly identified the minimum of J (in a simple binary model containing two rigid spheres; cf. LRS4, § 6.3) as a critical point in the evolution of contact systems. The orbital decay of a secularly unstable binary proceeds on the (de)synchronization timescale, which is typically much shorter than the timescale associated with any angular momentum loss mechanism (see LRS4, § 6). For two low-mass main-sequence stars with deep convective envelopes, this timescale could be as short as 10^4 yr (Zahn 1977). This may explain why the components of W UMa binaries are always observed to be in very shallow contact (Rucinski 1992). If the two components ever got closer together because of mass exchange or loss of angular momentum, the system would become secularly unstable and the two stars would quickly coalesce. The results of § 3 suggest that the degree of contact at the onset of secular instability is indeed small, at least for low-mass stars with mass ratio not too far from unity. The exact location of the secular stability limit (and the corresponding maximum value of the degree of contact for a stable, long-lived system) should depend sensitively on the internal structure of the binary, and, in particular, the distribution of specific entropy in the system. Thus a large sample of well-determined contact binary parameters could be used to place interesting constraints on their internal structure.

We have not explored the stability of mass transfer from one main-sequence star to another in this paper. This is in part because the simple polytropic model that we have adopted is not realistic enough. All our polytropic models would clearly lead to dynamically unstable mass transfer, independent of the mass ratio. In reality, mass transfer from one main-sequence star to another may be dynamically stable or unstable depending on the details of the internal structure of each component and the mass ratio. We did, however, present a complete calculation of dynamically unstable mass transfer for a *degenerate* system (§ 4.2), mainly to illustrate the differences between a dynamical coalescence driven by unstable mass transfer and one driven by a true dynamical instability of the binary equilibrium configuration. For two low-mass main-sequence stars, both instabilities can develop simultaneously, as demonstrated in § 4.1. The results of § 4.1 suggest that even when the mass transfer is dynamically stable, the orbital evolution of the binary may be affected by secular instabilities for sufficiently small mass ratio. If the Roche limit configuration is secularly unstable, mass transfer could be driven entirely by viscous dissipation, on a timescale much shorter than that of the angular momentum loss.

5.2. *Coalescence of Double White Dwarf Systems*

Our results show that hydrodynamics can play an important role in the coalescence of two white dwarfs, either because of dynamical instabilities of the equilibrium configuration (§ 3), or following the onset of dynamically unstable mass transfer (§ 4.2). Here also, a more detailed study of the stability of mass transfer between two white dwarfs in general would require the use of a more realistic equation of state. A calculation of dynamical mass transfer between two higher mass white dwarfs was performed by Benz et al. (1990) using a more realistic degenerate equation of state plus thermal gas pressure. Although the results of Benz et al. are qualitatively similar to ours, one may question their use of a nonequilibrium initial configuration. They started their calculation with two *spherical* stars, and with the secondary overflowing its critical lobe by almost 10% in radius. Not surprisingly, they found that the secondary was then tidally disrupted in less than an orbital period. In contrast, starting the calculation from a true equilibrium configuration (Figs. 11*a* and 12*a*) leads to a much more gradual increase in the mass transfer rate, and complete disruption of the secondary occurs only after several orbital periods during which the evolution is quasi-static.

For two massive enough white dwarfs, the merger product may be well above the Chandrasekhar mass $M_{\rm Ch}$. It may therefore explode as a (Type Ia) supernova, or perhaps collapse to a neutron star. The rapid rotation (cf. Fig. 6) and possibly high mass (up to $2M_{\rm Ch}$) of the object must be taken into account for determining its final fate. This is not done in current theoretical calculations of accretion-induced collapse (AIC), which always consider a nonrotating white dwarf just below the Chandra-

sekhar limit accreting matter slowly and quasi-spherically (Canal et al. 1990; Nomoto & Kondo 1991; Isern 1994). Under these assumptions it is found that collapse to a neutron star is possible only for a narrow range of initial conditions. In most cases, a (Type Ia) supernova explosion follows the ignition of the nuclear fuel in the degenerate core. However, the fate of a much more massive object with substantial rotational support and large deviations from spherical symmetry (as would be formed by dynamical coalescence) may be very different.

This work has been supported by a Hubble Fellowship to F. A. R. funded by NASA through grant HF-1037.01-92A from the Space Telescope Science Institute, which is operated by AURA, Inc., for NASA, under contract NAS5-26555. Partial support was also provided by NSF grant AST 91-19475 and NASA grant NAGW-2364 to Cornell University. F. A. R. also acknowledges the hospitality of the ITP at UC Santa Barbara. This research was conducted using the resources of the Cornell Theory Center, which receives major funding from the NSF and IBM Corporation, with additional support from the New York State Science and Technology Foundation and members of the Corporate Research Institute.

REFERENCES

Abramovici, A., et al. 1992, Science, 256, 325
Bailyn, C. D. 1993, in Structure and Dynamics of Globular Clusters, ed. S. G. Djorgovski & G. Meylan (ASP Conf. Ser., 50), 191
Bailyn, C. D., & Pinsonneault, M. H. 1994, ApJ, submitted
Bardeen, J. M., Friedman, J. L., Schutz, B. F., & Sorkin, R. 1977, ApJ, 217, L49
Benz, W., Bowers, R. L., Cameron, A. G. W., & Press, W. H. 1990, ApJ, 348, 647
Bodenheimer, P., & Ostriker, J. P. 1973, ApJ, 180, 159
Canal, R., Garcia, D., Isern, J., & Labay, J. 1990, ApJ, 356, L51
Chandrasekhar, S. 1969, Ellipsoidal Figures of Equilibrium (New Haven: Yale Univ. Press)
———. 1975, ApJ, 202, 809
Chen, K., & Leonard, P. J. T. 1993, ApJ, 411, L75
Colgate, S. A. 1990, in Supernovae, ed. S. E. Woosley (New York: Springer-Verlag), 585
Counselman, C. C. 1973, ApJ, 180, 307
Evans, C. R., Iben, I., & Smarr, L. 1987, ApJ, 323, 129
Hachisu, I. 1986, ApJS, 62, 461
Hachisu, I., & Eriguchi, Y. 1984a, PASJ, 36, 239
———. 1984b, PASJ, 36, 259
Hunter, C. 1977, ApJ, 213, 497
Iben, I., Jr., & Tutukov, A. V. 1984, ApJS, 54, 335
———. 1986, ApJ, 311, 753
Isern, P. 1994, in Evolutionary Links in the Zoo of Interacting Binaries, ed. F. D'Antona, Mem. Soc. Astron. Ital., in press
Kaluźny, J., & Rucinski, S. M. 1993, in Blue Stragglers, ed. R. A. Saffer (ASP Conf. Ser., 53), 164
Kippenhahn, R., & Weigert, A. 1990, Stellar Structure and Evolution (Berlin: Springer-Verlag)
Kopal, Z. 1978, Dynamics of Close Binary Systems (Dordrecht: Reidel)
Lai, D., Rasio, F. A., & Shapiro, S. L. 1993a, ApJS, 88, 205 (LRS1)
———. 1993b, ApJ, 406, L63 (LRS2)
———. 1993c, ApJ, 412, 593
———. 1994a, ApJ, 420, 811 (LRS3)
———. 1994b, ApJ, 423, 344 (LRS4)
———. 1994c, ApJ, in press (LRS5)
Leonard, P. J. T., & Clement, M. J. 1993, in Blue Stragglers, ed. R. A. Saffer (ASP Conf. Ser., 53), 193
Levine, A., Rappaport, S., Deeter, J. E., Boynton, P. E., & Nagase, F. 1993, ApJ, 410, 328
Livio, M., Pringle, J. E., & Saffer, R. A. 1992, MNRAS, 257, 15P
Mateo, M. 1993, in Blue Stragglers, ed. R. A. Saffer (ASP Conf. Ser., 53), 74
Mateo, M., Harris, H. C., Nemec, J., & Olszewski, E. W. 1990, AJ, 100, 469
Mathys, G. 1991, A&A, 245, 467
Nomoto, K., & Iben, I., Jr. 1985, ApJ, 297, 531
Nomoto, K., & Kondo, Y. 1991, ApJ, 367, L19
Ostriker, J. P., & Gunn, J. E. 1969, ApJ, 157, 1395
Paczyński, B. 1985, in Cataclysmic Variables and Low-Mass X-ray Binaries, ed. D. Q. Lamb & J. Patterson (Dordrecht: Reidel), 1
———. 1990, ApJ, 365, L9
Podsiadlowski, P., Pringle, J. E., & Rees, M. J. 1991, Nature, 352, 783
Rasio, F. A. 1993, in Blue Stragglers, ed. R. A. Saffer (ASP Conf. Ser., 53), 196
———. 1994, in Evolutionary Links in the Zoo of Interacting Binaries, ed. F. D'Antona, Mem. Soc. Astron. Ital., in press
Rasio, F. A., & Shapiro, S. L. 1992, ApJ, 401, 226 (RS)
———. 1994, ApJ, 432, 242 (Paper I)
Rucinski, S. M. 1992, in The Realm of Interacting Binary Stars, ed. J. Sahade et al. (Dordrecht: Kluwer), 111
Samec, R. G., Su, W., & Dewitt, J. R. 1993, PASP, 105, 1441
Shapiro, S. L., & Teukolsky, S. A. 1983, Black Holes, White Dwarfs, and Neutron Stars (New York: Wiley)
Shore, D., Livio, M., & van den Heuvel, E. P. J. 1994, Interacting Binaries (Berlin: Springer-Verlag)
Shu, F. H. 1980, in IAU Symp. 88, Close Binary Stars: Observationa and Interpretation, ed. M. J. Plavec, D. M. Popper, & R. K. Ulrich (Dordrecht: Reidel), 477
Shu, F. H., Lubow, S. H., & Anderson, L. 1976, ApJ, 209, 536
Stebbins, R. T., Faller, J. E., Hall, J. L., Hils, D., & Vincent, M. A. 1989, in Proc. 5th Marcel Grossman Meeting, ed. D. G. Blair & M. J. Buckingham (Cambridge: Cambridge Univ. Press), 1759
Tassoul, J.-L. 1978, Theory of Rotating Stars (Princeton: Princeton Univ. Press)
Tassoul, M. 1975, ApJ, 202, 803
Usov, V. V. 1992, Nature, 357, 472
van't Veer, F. 1979, A&A, 80, 287
Webbink, R. F. 1984, ApJ, 277, 355
Williams, P. S., & Roxburgh, I. W. 1976, MNRAS, 176, 81
Wolszczan, A. 1994, Science, 264, 538
Yan, L., & Mateo, M. 1994, ApJ, submitted
Yungelson, L. R., Livio, M., Tutukov, A. V., & Saffer, R. A. 1994, ApJ, 420, 336
Zahn, J.-P. 1977, A&A, 57, 383